



António Carranca de Almeida

Licenciatura em Engenharia de Micro e Nanotecnologias

Development of Graphene Based Supercapacitors

Dissertação para Obtenção do Grau de Mestre em
Engenharia de Micro e Nanotecnologias

Orientador: Professora Dr. Isabel Mercês Ferreira, Professora
Associada, FCT-UNL

Júri

Presidente: Dr. Rodrigo Ferrão de Paiva Martins, Professor Catedrático, FCT-UNL

Arguentes: Dr. Rui Manuel Marques Antunes, Professor Associado, IPS

Vogais: Dra. Isabel Mercês Ferreira, Professora Associada, FCT-UNL

Setembro de 2016

Development of Graphene Based Supercapacitors

Development of Graphene Based Supercapacitors

Copyright © António Carranca de Almeida, Faculdade de Ciências e Tecnologia, Universidade Nova de Lisboa.

A Faculdade de Ciências e Tecnologia e a Universidade Nova de Lisboa têm o direito, perpétuo e sem limites geográficos, de arquivar e publicar esta dissertação através de exemplares impressos reproduzidos em papel ou de forma digital, ou por qualquer outro meio conhecido ou que venha a ser inventado, e de a divulgar através de repositórios científicos e de admitir a sua cópia e distribuição com objetivos educacionais ou de investigação, não comerciais, desde que seja dado crédito ao autor e editor.

Development of Graphene Based Supercapacitors

Aos meus avós e à minha Titi, dedico a vocês...

Agradecimentos

Em primeiro lugar, gostaria de agradecer à Professora Dra. Isabel Ferreira, minha orientadora, que sempre demonstrou confiança e disponibilidade para todas as minhas dúvidas e questões, até as mais ridículas. Agradeço por todas as suas ideias e por todos os pensamentos de “porque não experimentar?” que nos fazem ver como realmente trabalha um investigador e nos inspira a trabalhar melhor.

Quero agradecer também ao Paulo Duarte que prescindiu de tanto do seu tempo livre para me ajudar em tudo o que precisei e que me motivou para fazer melhor em todas as fases desta tese. Se não fosse ele, esta tese não estava escrita.

Não posso deixar de agradecer a todos os membros da equipa: Inês, David, Catarina, Joana, Ju, Zeca, Joãozinho e Ana que sempre enaltecem o espírito de grupo e fizeram daquele laboratório um lugar espetacular para trabalhar! E ao Felipe, que tantas vezes parava de trabalhar para eu poder usar o laser.

Agradeço também ao Departamento de Conservação e Restauro por me deixarem usar o Raman e à Professora Dra. Susete Fernandes pela utilização da centrífuga.

Duas pessoas que não podem faltar são o Professor Dr. Rodrigo Martins e a Professora Dra. Elvira Fortunato. Este duo permitiu uma geração de engenheiros sonhar mais alto, mostrando ao mundo que não é necessário sair de Portugal para fazer coisas grandiosas.

Este é um culminar de uma fase e, por isso, estes agradecimentos são para todo o meu caminho neste curso que só foi possível por ter pessoas incríveis ao meu lado. Os meus pais são um grande exemplo disso. Agradeço ao meu pai que sempre me incentivou a fazer tudo e sempre me fez acreditar que tudo é possível, respondendo “Sim!” sem ver problemas e à minha mãe que, ao lado dele, é capaz de escrever uma lista enorme com todas as dificuldades que vou encontrar. Só com estes dois opostos é possível ter o exemplo perfeito: responder sim e logo de seguida ver todos os problemas que vou encontrar e como os resolver!

Agradeço às minhas irmãs, porque sem elas nada disto fazia sentido. Só elas me acompanharam desde sempre e me mostram todos os dias que nada faz sentido sem alguém para partilhar a felicidade. À minha irmã Madalena que mostra que todas as dificuldades são ultrapassáveis, mesmo que sejam doenças parvas como as nossas. À minha irmã Inês, que sempre mostrou que todas as discussões valem a pena se quiseres levar a tua a avante e que desistir não é uma solução. E à minha irmã Ana que sempre me motivou a estudar e a querer aprender tudo sem limites. Sem vocês isto não era possível.

Às minhas sobrinhas, um dos maiores agradecimentos de sempre porque, desde pequeninas, que me fazem trabalhar para ser melhor pessoa e um melhor exemplo e aos meus primos, que tanto me distraíram enquanto fazia a tese no grupo do whatsapp. Em especial ao Diogo e à Mariana que me apoiaram em todos os momentos mais difíceis e “me levaram na má vida”.

Nenhum agradecimento será maior que para os meus avós. O meu avô António, que não me vai chegar a ver engenheiro formado e que sempre me inspirou a ser o meu melhor eu a qualquer momento da minha vida. A minha Avó Olga que sempre me fez andar apresentável e bonito e quando não conseguiu, bem tentou! E à minha Titi, que mesmo sem ver esta fase final, mostrou que a resiliência de quem tem reais problemas na vida compensa e que desistir não é de facto uma opção viável. Dois deles partiram a meio desta tese e, como sempre quis que todos eles tivessem orgulho em mim, esta tese é dedicada a eles mesmo.

A todos os meus amigos da Faculdade, que sempre me acompanharam em todas as noites de estudo na 202 e todas as noites de loucura num bar! Em especial, ao Gabriel, claro. Sem ti o meu percurso académico tinha sido bem mais demorado e com muito menos piada. Todas as picardias e competições fizeram o impossível acontecer. Ao Jaime, porque sem ele seria completamente impossível ter passado a muitas cadeiras e tinham ficado muitas cervejas por beber. Ao Bruno que estando um ano à frente sempre me ajudou com todas as minhas dúvidas e todas as bebidas que não conseguia acabar. À Ana, que mesmo que não se lembre de mim em 4 anos, tornou-se uma amiga incrível e mostrou-me que não posso julgar um livro pela capa. E ao Pintinho, a pessoa que mais me acompanhou na faculdade e que desde do início sempre foi um grande amigo.

A todos os meus amigos de Loures que sempre compreenderam a minha ausência quando tinha de estudar e/ou fingir que estudava. Em especial à Mariana, que durante grande parte do meu curso me incentivou e motivou no sentido certo, fazendo-me estudar quando não me apetecia e, que mesmo com tudo o que passamos, mostrou-me que não é possível baixar os braços quando te sentes fraco ou desmotivado. Sempre foste um exemplo para mim de garra e perseverança. Obrigado por tudo.

This work was possible due to the partial financing support of the following projects: H2020-ICT-2014-1, RIA, TransFlexTeg-645241; ERC-CoG-2014, ChapTherPV, 647596; and by FEDER funds through the COMPETE 2020 Program and National Funds through FCT - Portuguese Foundation for Science and Technology under the project UID/CTM/50025/2013.

Abstract

The modern world is gasping for electrical energy, from our homes to our daily used devices such as phones, computers and even to our cars. Everything needs to be connected to a battery and the solution existent is becoming obsolete. The market is with a huge gap and supercapacitors are the answer for that space. Graphene assumes a role play in this field for its amazing surface area and its conductivity, making it a perfect candidate for the electrodes of this devices. In this work, two synthesis of graphene were produce: laser reduction of graphene oxide and electrochemical exfoliation of graphite.

The first one allows to develop patterns and build the devices in graphene oxide film, producing 2D supercapacitors. The geometry and the influence of the electrolyte were studied to maximize the capacitance. The graphene produced were analysed for its conductivity, quality and uniformity by CV curves, SEM and Raman Spectroscopy.

The electrochemical exfoliation allows to start from graphite and use a salt solution with application of voltage, which is an economic and safer alternative for producing graphene. Several concentrations of Na_2SO_4 were tested and all the material produced by this technique was characterized with Raman Spectroscopy, SEM and TEM images to evaluate the procedure.

Keywords: Graphene, Graphene Oxide, Supercapacitors, Laser reduction, electrochemical

Resumo

O mundo moderno está desesperado por energia elétrica, desde as nossas casas aos nossos dispositivos diários como telemóveis, computadores e até carros. Tudo precisa de estar conectado a uma bateria e a solução existente está a tornar-se obsoleta. O mercado tem uma lacuna enorme e supercondensadores são a resposta para esse espaço. O Grafeno assume um papel fundamental neste campo pela sua enorme área superficial e pela sua condutividade, tornando-o o candidato perfeito para os elétrodos destes dispositivos. Neste trabalho foram produzidas duas sínteses de grafeno: redução por laser e exfoliação eletroquímica da grafite.

A primeira permite desenvolver padrões e produzir dispositivos no filme de óxido de grafeno, criando supercondensadores 2D. A geometria e a influência do eletrólito foram estudadas para maximizar a capacitância. O grafeno produzido foi analisado à sua condutividade, qualidade e uniformidade com curvas CV, SEM e Espectroscopia de Raman.

A exfoliação eletroquímica permite começar com grafite e usar uma solução de sal com aplicação de tensão, que é uma maneira mais económica e segura de produzir grafeno. Várias concentrações de Na_2SO_4 foram testadas e todo o material produzido por esta técnica foi caracterizado com Espectroscopia de Raman e imagens de SEM e TEM para avaliar este procedimento.

Palavras-Chave: Grafeno, Óxido de Grafeno, Supercondensadores, Redução por laser, eletroquímico

Contents

Agradecimientos	v
Abstract	vii
Resumo	ix
List of Tables	xiii
List of Figures	xv
Abbreviations	xvii
Motivation and Objectives	xix
1 Introduction	1
1.1 Graphene	1
1.1.1 <i>Synthesis</i>	2
1.2 Supercapacitors	3
1.2.1 <i>Electrodes</i>	4
1.2.2 <i>Electrolytes</i>	4
2 Materials and Methods	5
2.1 Production Methods	5
2.1.1 <i>Synthesis of GO films</i>	5
2.1.2 <i>Laser Reduction of GO films</i>	5
2.1.3 <i>Electrochemical Synthesis of few layer graphene</i>	5
2.1.4 <i>Electrolytes</i>	6
2.2 Characterization Methods.....	6
2.2.1 <i>Resistivity measurements</i>	6
2.2.2 <i>Capacitance measurements</i>	6
2.2.3 <i>Raman microscopy</i>	6
2.2.4 <i>Morphology analysis</i>	6
2.2.5 <i>Optical Microscopy</i>	6
3 Results and discussion	7
3.1 Graphene Oxide Laser Reduction	7
3.1.1 <i>Influence of Laser Parameters</i>	7
3.1.2 <i>Power influence</i>	8
3.1.3 <i>Scanning speed and Frequency influence</i>	10
3.1.4 <i>Morphological characterization</i>	12
3.1.5 <i>Laser lines definition</i>	13
3.2 Capacitors.....	13
3.2.1 <i>Geometry influence</i>	14

Development of Graphene Based Supercapacitors

3.2.2	<i>Electrolyte influence</i>	15
3.3	Electrochemical synthesis	18
4	Conclusions and Future Perspectives	25
	References	27

List of Tables

Table 3.1 - Conductivities and Raman spectra's ratio for each power.	9
Table 3.2 - Conductivities and Raman Spectra's Ratios for each speed and frequency.	11
Table 3.3 - Influence of the geometry in the specific capacitance of the device with different scan rates (capacitance in $\mu\text{C}/\text{mm}^2$).....	15
Table 3.4 - Test results of the electrolytes at different scan rates (capacitance in $\mu\text{C}/\text{mm}^2$).....	17
Table 3.5 – Raman Shift Peaks of all samples (peak position in cm^{-1}).	19

List of Figures

Figure 1.1 - Raman scattering spectra for different carbon based materials. Adapted from [35].	1
Figure 1.2 - a) Graphite structure. b) Graphene oxide with highlighted functional groups. c) Reduced Graphene Oxide with highlighted functional groups. [19]	2
Figure 1.3 - Simplified Ragone plot of the energy storage domains for the various electrochemical energy conversion systems compared to an internal combustion engine and turbines and conventional capacitors. [26]	4
Figure 1.4 - Schematic of an electrochemical double-layer capacitor. [25]	4
Figure 2.1 - Schematic of the devices' design.	5
Figure 3.1 - Microscope Image of a) rGO S21, P3, F2500 and b) rGO S21, P8, F2500.	7
Figure 3.2 - Conductivity vs Power for each scanning speed (28,19,20,21,22) and frequency, 2000 a), 2500 b) and 3000 c).	7
Figure 3.3 - Microscopy images of rGO obtained with the laser conditions of: a) S21, P4, F2500; b) S21, P5, F2500; c) S21, P6, F2500; d) S21, P7, F2500.	8
Figure 3.4 - Raman Spectra of different powers with fixed S, 21 and F, 2500.	9
Figure 3.5 - Microscope Image of rGO obtained at P5 with: a) S18 F2500; b) S19 F2500; c) S20 F2500; d) S21 F2500; e) S22 F2500; f) S21 F2000; g) S21 F3000.	10
Figure 3.6 - Raman shifts of each Speed, a), and each frequency, b).	11
Figure 3.7 - SEM Image of GO, a) and b), and rGO, c) and d).	12
Figure 3.8 - a) Several laser traces thicknesses ranging from 0.01 mm to 0.1 mm with a step of 0.1 mm at 5% power b) smallest thickness well defined with a 5% power.	13
Figure 3.9 - Geometries of the tested capacitors.	13
Figure 3.10 - CV curves of the four different geometries: a) Parallel Lines, b) Circular, c) Interdigital Small and d) Interdigital Large.	14
Figure 3.11 - CV curve of base line without electrolyte.	15
Figure 3.12 - CV curves of each electrolyte used: a) CMC AC PC; b) CMC NP; c) KOH; d) IL NP.	16
Figure 3.13 - Specific Capacitance of every electrolyte vs scan rate.	17
Figure 3.14 - IL NP CV curves a) Initial b) after a month.	18
Figure 3.15 - Raman shift of the Electrochemical synthesis's powders obtained with sea water and Na ₂ SO ₄ solutions of 0.5M; 0.3M; and 0.1M.	19
Figure 3.16 - Raman spectra's ratios for each Electrochemical sample and the initial graphite.	20

Figure 3.17 - Deconvolution of Raman Spectra 2D peaks through Lorentz Fit of powder created from: a) Starting Graphite; b) Sea Water; c) 0.1M; d) 0.3M; and e) 0.1M. 20

Figure 3.18 - SEM images of the powders produced 21

Figure 3.19 – a) and b) TEM images with different magnification, of exfoliated powder with 0.1M Na₂SO₄ solution c) EDS analysis of the same powder..... 22

Figure 3.20 - a) and b) TEM image of exfoliated powder with 0.3M Na₂SO₄ solution c) EDS analysis of the same powder..... 23

Figure 3.21 - a) and b) TEM image of exfoliated powder with 0.5M Na₂SO₄ solution c) EDS analysis of the same powder..... 24

Abbreviations

- AC – Cellulose Acetate
- CMC – Carboximethyl cellulose
- CV – Cyclic Voltammetry
- CVD - Chemical Vapour Deposition
- EDLC – Electrochemical double-layer capacitor
- EDS - Energy Dispersive Spectroscopy
- F - Frequency
- GO – Graphene Oxide
- IL – Ionic Liquid
- P - Power
- PC – Propylene Carbonate
- rGO – reduced Graphene Oxide
- S – Speed
- SEM - Scanning Electron Microscopy
- TEM - Transmission Electron Microscopy

Motivation and Objectives

Nowadays, living in a modern technologic world, the urge for better ways to store and transport energy is increasing. New and more electronic products are being consumed and it's starting to reach every sector of the society, from mobile phones to cars. This necessity creates a void in the market and researchers are pressured to come up with an alternative to the obsolete solution in use.

Supercapacitors present the best alternative, allowing to obtain greater energy densities while maintain the power density of the conventional capacitors. This means that, when compared with regular batteries, the time consumed in the charging process for supercapacitors can be lower and, therefore, allowing devices to unplug the wall socket. The devices that already exists lacks the energy density necessary, usually 3 to 30 times lower than conventional batteries and, consequently, further studies have to be made improve this aspect. [1]

Graphene emerge as a super material and as being linked to many fields' studies, from transparent protective coatings to electronics.[2] With amazing properties, this material promise to revolutionize several areas and supercapacitors seems to be one of them, due to its high surface area.

The main objective of this work is to produce these devices with high throughput using environmentally friendly methods and, with that in focus, it was divided in several studies:

- Optimization of the laser parameters for the graphene oxide reduction
- Production of an all solid-state supercapacitor
- Production of few-layers graphene by a more environmentally friendly and affordable method

1 Introduction

The supercapacitors have been facing a huge development in the last years, with many configurations and materials studied [1]. In this thesis, planar graphene based capacitors were developed and characterized.

1.1 Graphene

Graphene is considered as an excellent candidate material to be used as electrodes in supercapacitors do to its amazing properties (high surface area, high electrical conductivity, abundant material, high performance with low quantity of material) that rivals with in-plane values of graphite.

Graphene is a carbon based compound arranged in a hexagonal bi-dimensional honeycomb lattice.[3] There are two types of bonds on the crystal lattice, one strong, bond σ , and the other one weak, π bond. The first one is formed by the hybrid orbitals sp^2 , created by the combination of $2p_x$ and $2p_y$ with the $2s$ orbital, and give the 6-atom cell covalent bonds between the atoms. The π bonds are formed by the $2p_z$ of each atom combined with the respective from the adjacent layer. [4]

The Raman Spectroscopy is an excellent tool to access the existence or not of these bonds. Three main bands can be observed in the Raman spectra of carbon based materials, when it is excited with a 532 nm laser: D band at $\sim 1350\text{ cm}^{-1}$; G band at $\sim 1580\text{ cm}^{-1}$ and 2D band at $\sim 2690\text{ cm}^{-1}$, as seen in Figure 1.1. [3] Each one of them can be linked to a specific crystallographic property: D band and G band are

connected to two primary in-plane vibrational modes and 2D to a second order overtone of D. [3]

This new material is in the spotlight for its amazing theoretical properties such as high intrinsic mobility of $2 \times 10^5\text{ cm}^2\text{ V}^{-1}\text{ s}^{-1}$ [2] and a specific surface area of $2630\text{ m}^2\text{ g}^{-1}$ [5], between others [3]–[5]. Such properties can only be achieved in small samples or in specific substrates [2] and therefore cannot be seen as a given fact but their existence made graphene a material capable for a wide range of applications in electronics. [9]–[12]

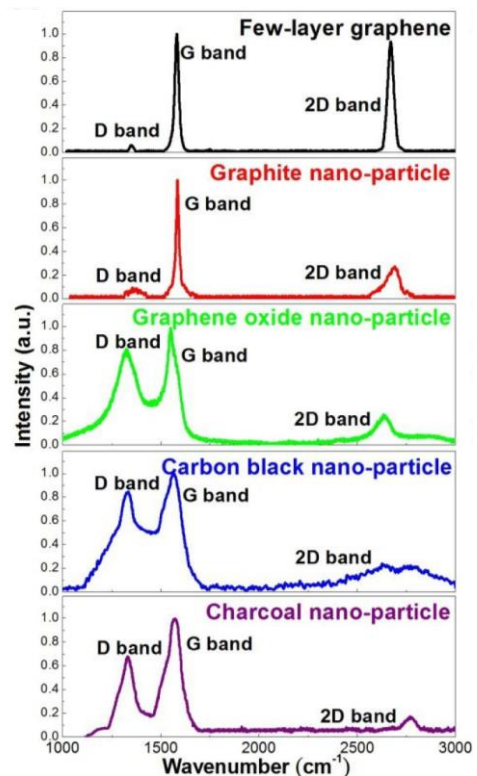


Figure 1.1 - Raman scattering spectra for different carbon based materials. Adapted from [35].

1.1.1 Synthesis

Graphene has been obtained mainly by chemical vapor deposition (CVD)[13] or mechanical exfoliation of bulk graphite.[14] Single-layer transferable graphene nanosheets of high purity can be obtained, but these techniques have some limitations and are less effective for large-scale production. Chemical synthesis is the most promising method for the industrial production of graphene-like materials.

One way to produce graphene is by chemical reduction of synthesised Graphene Oxide (GO). The production of this material is being study since 1859 and three methods emerge: Brodie [15], Staudenmaier [16] and Hummers [17], all of them using fuming acids to oxidize the graphite layers and obtaining GO. This method allows to create a layered material of oxygenated graphene sheets bearing oxygen functional groups on their basal planes and edges, as demonstrate in Figure 1.2 . [18] These groups make graphene oxide hydrophilic but with the redraw of its lateral size being usually few tens of micrometres. [19]

The Reduced Graphene Oxide (rGO), can be obtained via a reduction of Graphite Oxide and this can be achieved by several different ways [20]–[22], one of which is Laser reduction. In this technique, a low power laser, between 1 and 4W, is applied to a film of graphene oxide. [23] This offers, in comparison to the conventional photolithography, a cheaper, faster and with a higher throughput way to produce 2 dimensional devices, such as supercapacitors in a graphene oxide film and also has the advantage of not using toxic chemicals typically used in chemical reduction process.[23] Another possible and advantageous process is the exfoliation of graphite by electrochemical method. In the state of the art few works have already proved this possibility, using metal and graphite electrodes or just graphite electrodes to obtain few layer graphene. [19], [24]

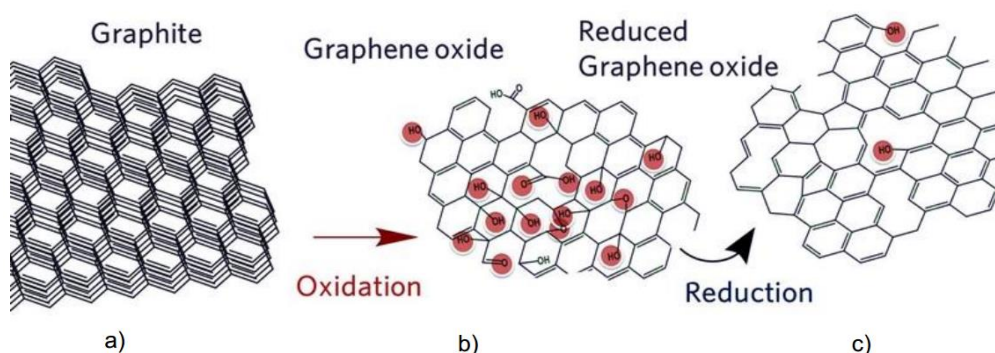


Figure 1.2 - a) Graphite structure. b) Graphene oxide with highlighted functional groups. c) Reduced Graphene Oxide with highlighted functional groups. [19]

1.2 Supercapacitors

A capacitor is a device where two conducting electrodes are separated by an insulating dielectric material. If a potential difference is applied to the terminals of the capacitor, opposite charges accumulate on the surface of each electrode. This stores energy by producing an electric field because charges are kept away with the dielectric barrier.[25]

The capacitance of the device can be calculated from the ratio of stored charge, Q , and the applied voltage or the area of each electrode, A , times the permittivity, $\epsilon_0 \cdot \epsilon_r$, of the dielectric layer divided by the thickness of the last, d . [25]

$$C = \frac{Q}{V} = \epsilon_0 \cdot \epsilon_r \cdot \frac{A}{d} \quad (1)$$

According to the above equation, the capacitance is proportional to the area of the capacitor. Therefore, it can be enhanced by increasing largely the dimension of the capacitor or increasing largely the surface area. Supercapacitors fill this condition, very high surface area leads to very high capacitance and in some cases, it also works with electrolytes. These are a new type of devices that fill a hole between the batteries and capacitors. They can compete with capacitors in specific power and, at the same time, have a specific energy capable of overlap some of the batteries, as showed in Figure 1.3. [26]

Supercapacitors are ruled by the same physical principals as conventional capacitors. However, by using electrodes with much higher surface area and thinner dielectrics, these devices can achieve much higher capacitances.[25]

Electric Double Layer Capacitors (EDLCs) are specific supercapacitors that accumulate charges at the interface between electrodes and electrolyte. As shown in Figure 1.4, the accumulated charges form two electric double-layers, one on each interface, and the surface area of the electrode plays a huge role in the device's capacitance. [27] This capacitance can be estimated by the Helmholtz model proposed in 1853:

$$\frac{C}{A} = \frac{\epsilon}{4\pi\delta} \quad (2)$$

In this model, C is the capacitance, A is the surface area, ϵ is the relative dielectric constant of the electrolyte and δ is the distance between the electrode and the centre of the ion layer, typically a few angstroms. [27]

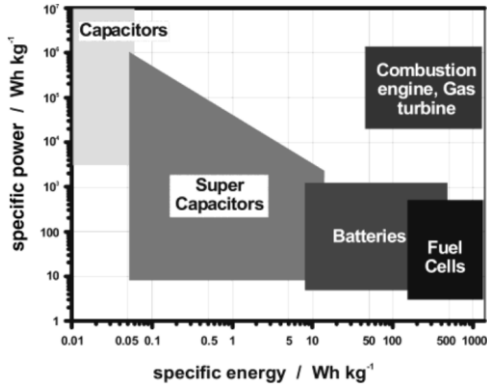


Figure 1.3 - Simplified Ragone plot of the energy storage domains for the various electrochemical energy conversion systems compared to an internal combustion engine and turbines and conventional capacitors. [26]

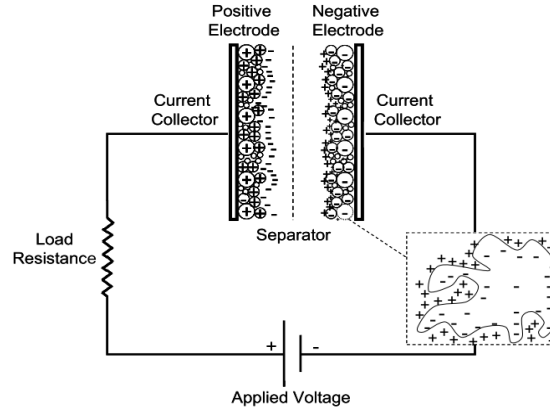


Figure 1.4 - Schematic of an electrochemical double-layer capacitor. [25]

1.2.1 Electrodes

As already mentioned in the previous section, the surface area of the electrode can play a great influence in the capacitance. Therefore, graphene emerges as an important candidate for electrodes because its large surface area and a 2D geometry of those electrodes can further improve the capacitance. [6,22,23,28,29] Interdigital geometry seems to be an obvious choice but are others such as plates and circular that can improve the capacitance of the device.

1.2.2 Electrolytes

Since electrolyte is required to create a double-layer in the electrode surface, this component require specific characteristics. One of the most important is the ions size of the electrolyte. This influences their mobility within the electrode and the respective insertion/removal which also depends on the porosity of the electrodes, affecting consequently the response time of the device. [30]

The solid electrolyte and gel electrolytes are important improvements over liquid one, for producing devices more compact, more reliable, environmentally safe and with long shelf life.[31] However in polymeric solid electrolyte ion movements are much slower than in liquids and, the capacitance of the device is affected negatively. Therefore, although it is important to replace electrolytes fluids to solids, a compromise between the advantages of these and the loss of capacity of the devices is necessary.

2 Materials and Methods

2.1 Production Methods

2.1.1 Synthesis of GO films

To produce the GO powder, a modified Hummer method was used as reported elsewhere. [17]. The GO was dispersed in water with a concentration of 5 mg/mL and tip sonicated in a MSK-USP-3N Ultrasonic for 4 hours, in an ice bath, with 1 minute ON/1 minute OFF cycles, to create a stable dispersion. The sonicated dispersions were then drop casted in 3.5 cm² boxes with a previously cut glass substrate with the same dimensions. The volume was kept constant at 5 mL per box to produce uniform films of GO.

2.1.2 Laser Reduction of GO films

The electrode geometry designs were created in Corel Draw X7. As showed in Figure 2.1, four designs were produced and tested: two interdigital devices with different fingers thickness and spacing; two simple parallel plates and a circular one. The devices were printed in a 40W Epilog Laser Mini. Three parameters were studied in this process: power (P), speed (S) and frequency (F) of the laser. For the conductivity tests, 5 mm by 1 mm traces were made with combinations of the three parameters with three replications for each sample.

Laser minimum definition was performed printing 10 lines starting from 0.01 mm with a step of 0.01 mm.

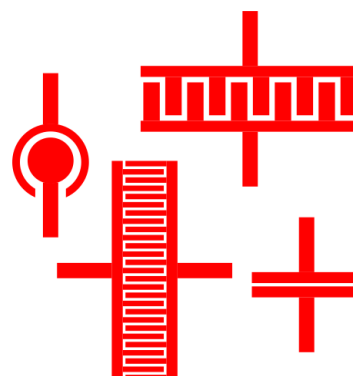


Figure 2.1 - Schematic of the devices' design.

2.1.3 Electrochemical Synthesis of few layer graphene

Two rods of commercial Graphite were submerged in a goblet with sea water and an aqueous solution of Na₂SO₄ with 3 different concentrations: 0.1M, 0.3M and 0.5M. Using a power supply, 10 V were applied between the rods separated by 1.5 cm for 5 minutes. The reaction products were then washed 4 times by centrifugation with water to remove the salt.

2.1.4 Electrolytes

In order to evaluate the influence of the electrolyte into the capacitance of the produced devices, four different electrolytes were tested, two liquids and two solids. The liquid electrolytes were 1M of aqueous solution of KOH and a mixture of 0.03 g SiO₂ nanoparticles with 1 g of ionic liquid (IL) 1-Butyl-3-methylimidazolium bis(trifluoromethylsulfonyl)imide (Sigma-Aldrich). The solid electrolytes used was CMC-AC-PC (0.384 g of cellulose acetate (AC) and 0.207 g of liquid propylene carbonate (PC) were stirred for 2 hours in 50 mL of deionized water. 2 g CMC were then added to the solution and stirred for more 48 hours to ensure a good homogeneous solution) and CMC NP (0.06 g SiO₂ nanoparticles were stirred for 2 hours in 50 mL of deionized water. 2 g CMC were added to the solution and stirred for more 48 hours to ensure a good homogeneous solution).

2.2 Characterization Methods

2.2.1 Resistivity measurements

To determine the resistivity of the rGO obtained by laser reduction, IV curves using a Keithley Picoammeter/Voltage were performed and repeated three times for each sample.

2.2.2 Capacitance measurements

The supercapacitors created were characterized in a Reference 3000 Potentiostat using cyclic voltammeteries sweeps from 0 to 1 V with a step of 5mV at 5 different scan rates: 40 mV/s, 80 mV/s, 120 mV/s, 160 mV/s and 200 mV/s. The specific capacitance was calculated using the software Gamry Echem Analyst.

2.2.3 Raman microscopy

Raman microscopy was carried out at the Department Conservation and Restoration (FCT-UNL) using a Labram 300 Jobin Yvon spectrometer, equipped with a solid-state laser operating at 532 nm. The laser beam was focused with 50× Olympus objective lens and spectra were recorded.

2.2.4 Morphology analysis

The surface morphology of GO, rGO and electrochemical G samples was obtained by scanning electron microscope. The TEM analysis were made with a Hitachi 8100 with LaB6 filament. Both equipment are in MicroLab-Electro Microscopy Laboratory of IST.

2.2.5 Optical Microscopy

The surface of the reduced film was observed in an inverted optical microscope Leica DMi8, at Lab 213 at DCM – FCT-UNL.

3 Results and discussion

In this section the results of rGO obtained by laser and the G obtained by electrochemical synthesis are presented and discussed.

3.1 Graphene Oxide Laser Reduction

The reduction of graphene oxide can be performed by several techniques but in this thesis the reduction by Laser was the one tested and used to perform the supercapacitors. To achieve good quality rGO a preliminary study had to be performed in order to define how the laser parameters such as power, scanning speed and frequency of pulse influence the electrical properties of rGO films obtained.

3.1.1 Influence of Laser Parameters

Preliminary tests, were performed by trial and error attempts at the laser's power until finding out the a rGO area. The boundaries were found at P3 and P8, as shown in Figure 3.1. In the first case,

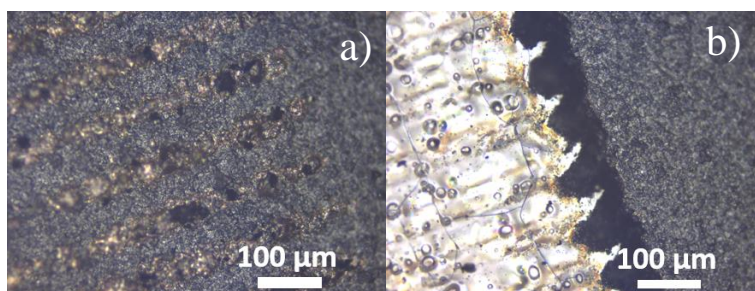


Figure 3.1 - Microscope Image of a) rGO S21, P3, F2500 and b) rGO S21, P8, F2500.

a), almost none of the GO were reduced, leaving marks of the laser but with no uniformity or even connections between those marks. The P8 removed the film completely, leaving behind some marks of the laser in the glass substrate.

In order to determine the right parameters to reduce the GO, the conductivities values were analysed and plot in the Figure 3.2. The thickness of the film was measured with a digital micrometre and used in every sample from this point forward as 17.25 μm . As can be seen, the

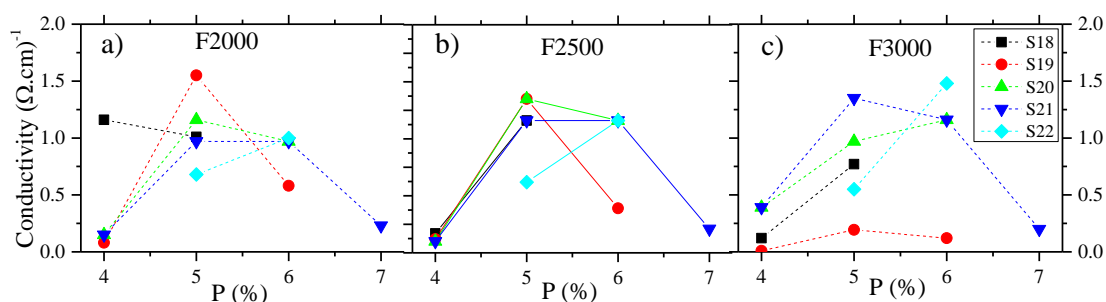


Figure 3.2 - Conductivity vs Power for each scanning speed (28,19,20,21,22) and frequency, 2000 a), 2500 b) and 3000 c).

combination of scanning speed, power and frequency are important to maximize the outcome conductivity of rGO. Independently of frequency and scanning speed used, the power of 5 and 6 gives always better conductivities. In Figure 3.2 c), can be seen that for the same power by combining scanning speed and frequency the conductivity values can be optimized. In general, for lower frequencies, low scanning speeds are needed to optimize the conductivity of rGO. There is a direct interdependence between speed and frequency which was expected since for lower frequencies the laser beam needs to be longer at the same position to irradiate similar quantity of energy to the GO film.

Overall, with this study we were able to define the laser parameters to obtain high conductivity rGO: power should be between 5 and 6 and frequency can be any of the tested values if the scanning speed is chosen correctly. In the following we analyse the influence of each parameter.

3.1.2 Power influence

The rGO zones obtained for some of the laser parameters tested and presented before were observed in a microscope. Keeping the speed and frequency at 21 and 2500, lines for the four powers were made and microscopy images of the obtained lines are shown in Figure 3.3. For P4, in Figure 3.3 a), there are visible parts of the film not reduced, showing lighter colours in the line area. In Figure 3.3 d), an obvious overexposure leaves almost all white colour from the light passing through the glass. In the other two, a uniform film created can be seen, although some spots of light are still visible. This can be attributed to an eventually thinner part of the film or even to a peel-off after the exposure of the laser.

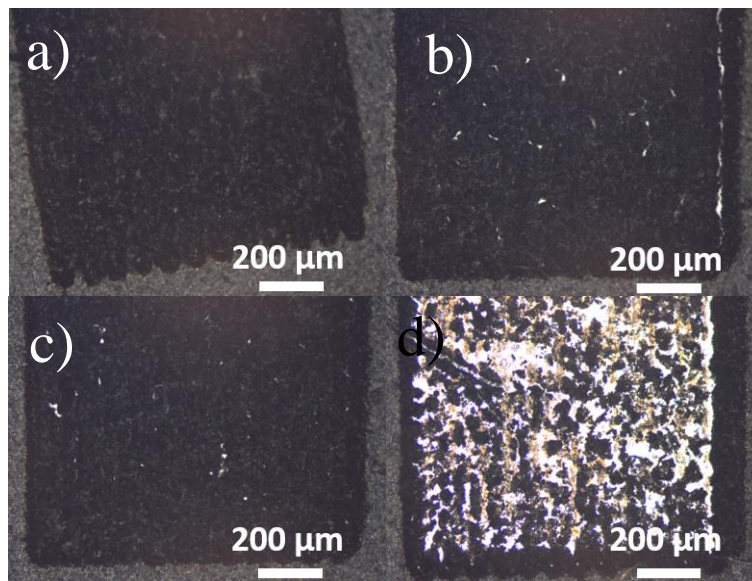


Figure 3.3 - Microscopy images of rGO obtained with the laser conditions of: a) S21, P4, F2500; b) S21, P5, F2500; c) S21, P6, F2500; d) S21, P7, F2500.

The images of Figure 3.3 are in agreement with the values of Figure 3.2 for the corresponding experimental conditions. That is, the best conductivities (values in table 3.1) were obtained for P5 and P6 images b) and c), respectively.

The Raman Spectra of the initial GO and rGO films obtained for the different Power conditions are plotted in Figure 3.4. The analysis of Raman spectra and its relation with the graphene, reduced graphene oxide and graphene oxide have been presented in the literature. However, as graphene is obtained by several methods, its characteristics in terms of defects, oxidation, number of layers are quite different from method to method. In general, a sharp and high intensity 2D band at 2690 cm^{-1} has been attributed to graphene and related to double phonon scattering (either both on a single electron/hole or on an electron-hole pair). [32], [33] An increase in the number of layers in graphene do shift this band to higher wavenumbers. On the other hand, for disorder or defected graphene the enhancement of D band is observed. As such, the obtained Raman spectra show graphene-like material after laser reduction of GO and the laser power does not influence remarkably the intensity of these peaks, although some differences in the ratio of I_D/I_G and I_{2D}/I_G are seen (table 3.1). These observed differences between rGO samples do not have a correlation with the laser power used, meaning that in this range of values it does not influence the quality of rGO, but since micro Raman just analyses a small portion of the material the differences observed can mean solely a variation along the sample of rGO film produced. The comparison of the Raman spectra with that of synthesised GO film clearly evidence the existence of graphene-like material. The GO spectrum reveals a lack of 2D band and a much higher D band, due to the fact that functional groups increase the number of defects in the film. With a relative height of 0.926, the D band have, with negligible difference, the same intensity of G band in this material. On the other hand, each sample of rGO shows a decrease in defects and the appearance of 2D confirms the good reduction of the GO.

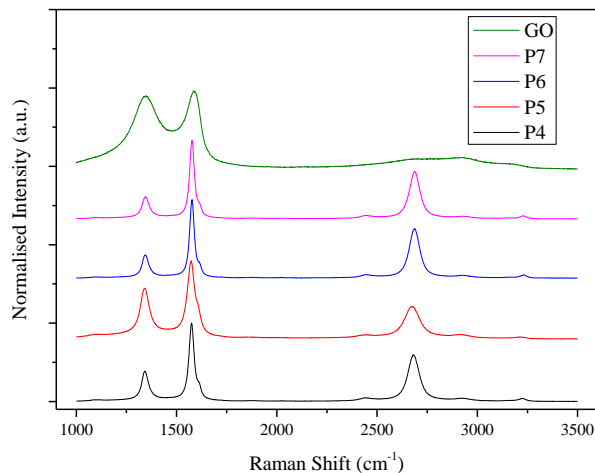


Figure 3.4 - Raman Spectra of different powers with fixed S, 21 and F, 2500.

Table 3.1 - Conductivities and Raman spectra's ratio for each power.

<i>Power</i>	Conductivity $(\Omega.\text{cm})^{-1}$	Raman	
		I_D/I_G	I_{2D}/I_G
4%	0.16	0.387	0.594
5%	1.74	0.648	0.417
6%	1.74	0.296	0.629
7%	0.21	0.284	0.603

3.1.3 Scanning speed and Frequency influence

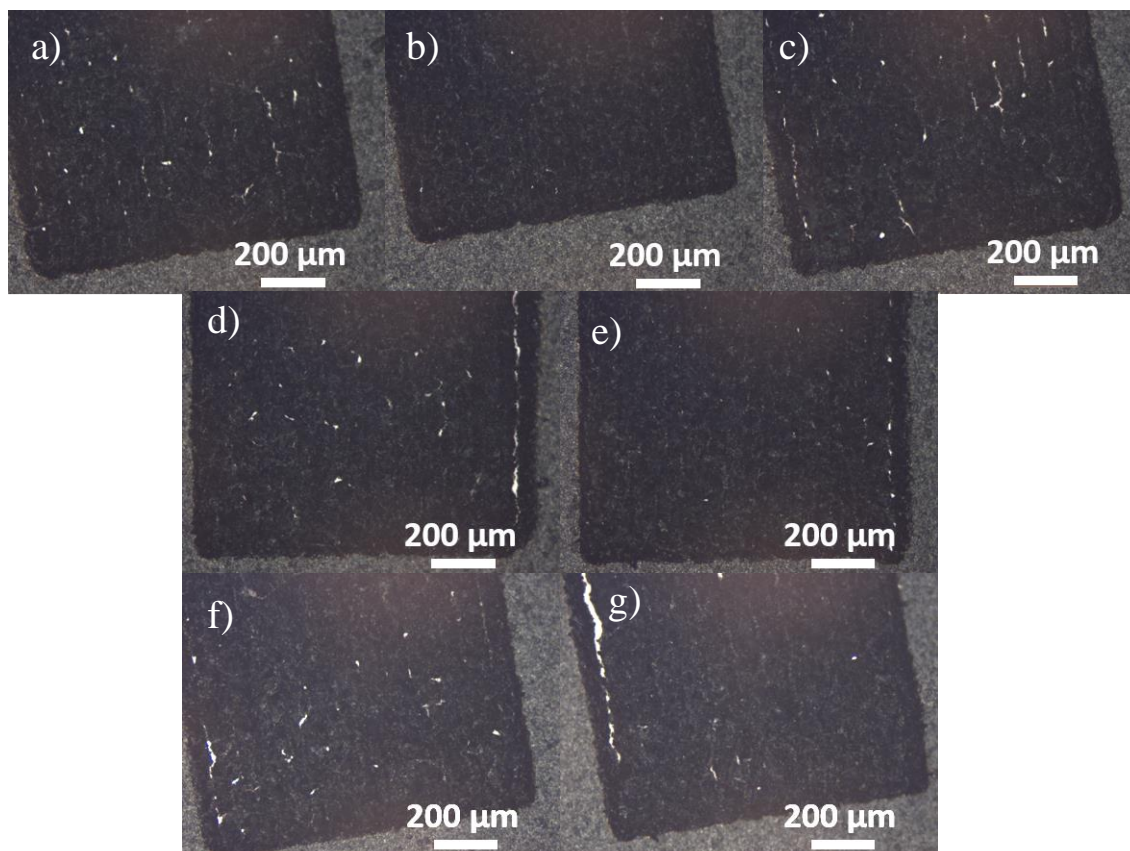


Figure 3.5 - Microscope Image of rGO obtained at P5 with: a) S18 F2500; b) S19 F2500; c) S20 F2500; d) S21 F2500; e) S22 F2500; f) S21 F2000; g) S21 F3000.

Analysing the microscope images, one can notice that all of them present a suitable level of reduction with small imperfections that can be caused, as previously said, due to a thinner part of the GO film or even to an eventually peel-off of the material after the exposure. This confirms the lower influence speed and frequency has in the reduction of the GO, at least by microscopy observation.

Similar conclusion can be taken from Raman spectra for samples processed with different scanning speed. In the Figure 3.6 a), the plots are all similar, with negligible deviations of the peaks' position. No shift is seen in any sample and the mean of conductivities prove this observation, as the same value was measured for every sample, $1.16 (\Omega \cdot \text{cm})^{-1}$, except the fastest, S22, that was almost half. The non-uniformity of samples could be responsible for this small variation and so, these parameters in this range of variation do not need fine tune to obtain optimized rGO films. Comparing with the GO, the same result is observed. Less defects in every sample and presenting a 2D band, proving the good reduction of the film.

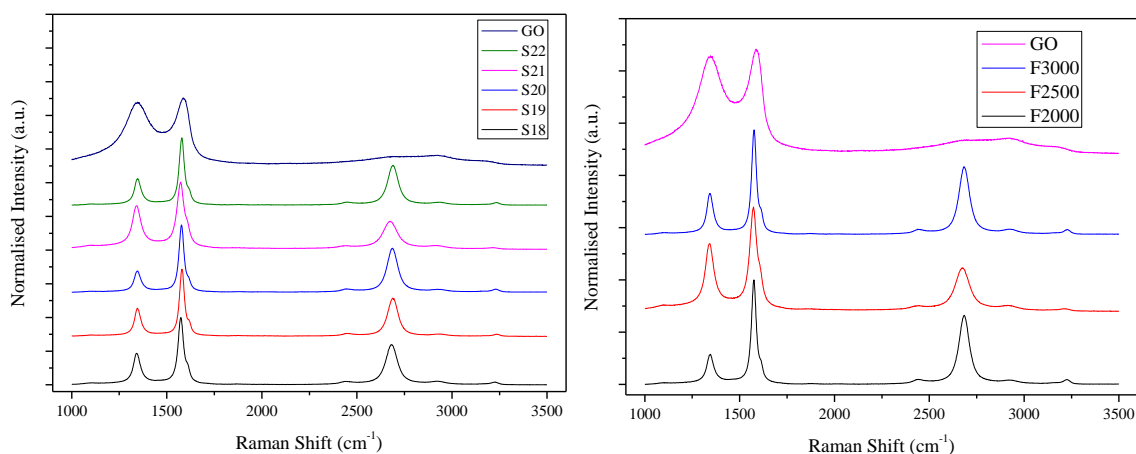


Figure 3.6 - Raman shifts of each Speed, a), and each frequency, b).

In the Raman Spectra of Figure 3.6 b), a small variation can be seen in the heights of the normalised peaks D and 2D. As said previously, this can vary from samples to sample and from the spot chosen to focus the laser and the comparison with GO reveals, once again, a good reduction of the film. The variation of the conductivity follows the same pattern, as shown in Table 3.2, meaning that frequency also doesn't show a need for fine tune in this range of variation.

Table 3.2 - Conductivities and Raman Spectra's Ratios for each speed and frequency.

<i>Speed</i>	<i>Frequency</i>	<i>Conductivity ($\Omega.cm$)⁻¹</i>	<i>Raman</i>	
			I_D/I_G	I_{2D}/I_G
18%	2500	1.16	0.468	0.599
19%	2500	1.16	0.417	0.567
20%	2500	1.16	0.315	0.653
21%	2500	1.16	0.648	0.417
22%	2500	0.62	0.387	0.590
21%	2000	1.55	0.288	0.660
21%	3000	1.35	0.391	0.645

3.1.4 Morphological characterization

The figure 3.9 contains the SEM images of both GO and rGO films obtained for P5, F2500 and S19 with two magnifications. The surface morphology of GO (figure 3.9 a) and b)) is composed by uniform distribution of flakes along the sample. The magnification image shows dense and interconnected flakes leading to a compact film.

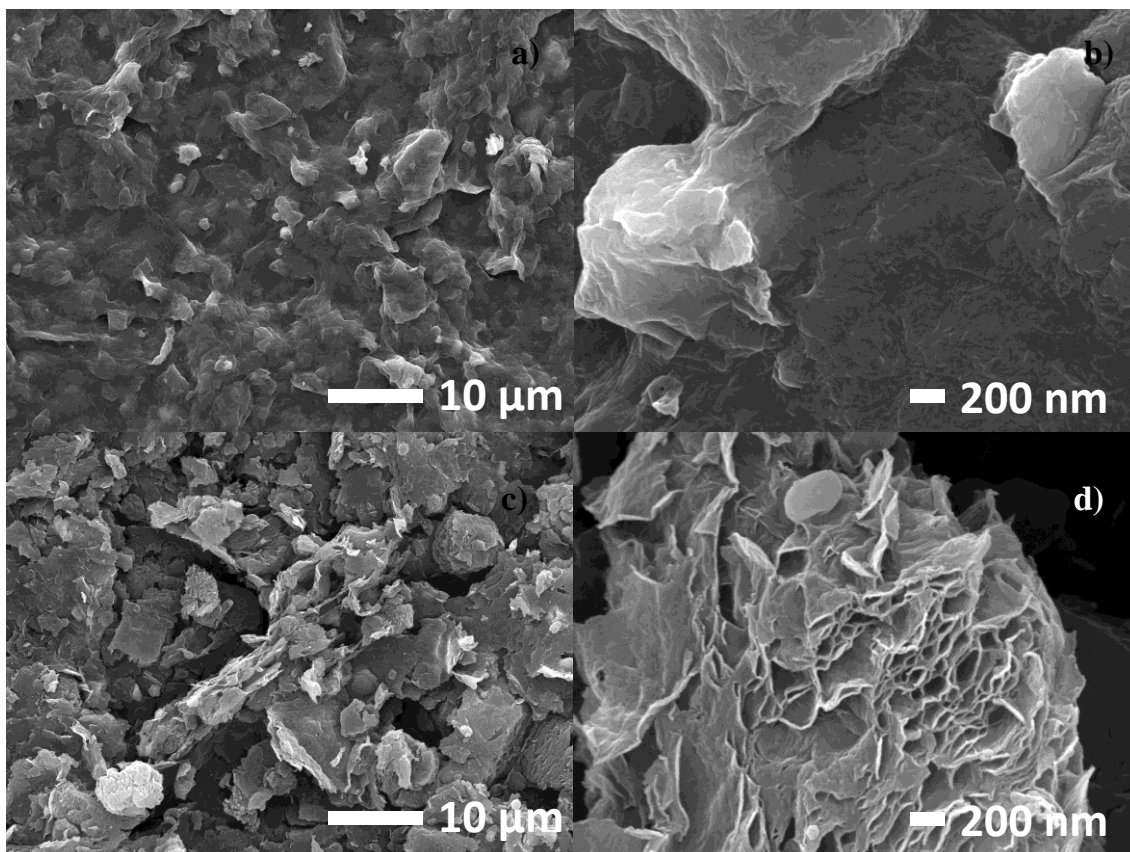


Figure 3.7 - SEM Image of GO, a) and b), and rGO, c) and d).

After the reduction, the film is quite distinct from its precursor, figure 3.9 c) and d). The exposure to laser of GO leads to small structures like micro grains appearing in the SEM image with less magnification with an apparent high surface roughness compared to GO. At the higher magnification scale, it is clearly seen the micro grains formed by foils separated by empty space. So, graphene foils are formed although they are corrugated and form micro-blocks of graphite. This agrees with the Raman results since, a mixture of graphene, graphite and oxygen/voids are shown by the peaks obtained. However, these were the expected results, GO single foils are very difficult to obtain by Hummers method. Even if a good exfoliation is obtained, the formation of GO films by drop casting and subsequent drying promotes again the foils aggregation and the rGO film is then formed by grains of corrugated graphene sheets.

Overall, the rGO obtained by the laser exfoliation lead to films with high conductivity and high surface area and they should be adequate to be applied in supercapacitors. Here it is important to highlight that for the capacitors geometries to be study, the minimum laser line and line separations should be identified, and so the following study was performed.

3.1.5 Laser lines definition

Choosing the best laser parameters in Figure 3.8 a), it is observed the 5 lines that were produced. The smallest width with no cuts and with negligible anomalies that don't compromise the conductivity of the line is around 90 μm . This value is only an approximation because, as can be seen in the Figure 3.8 b), the value differs along the line. Therefore, to ensure a homogenous reduction of the film, at least 100 μm should be used. It is important to know this limit size for the design of the devices, showing that the minimum possible for a finger is at least that value.

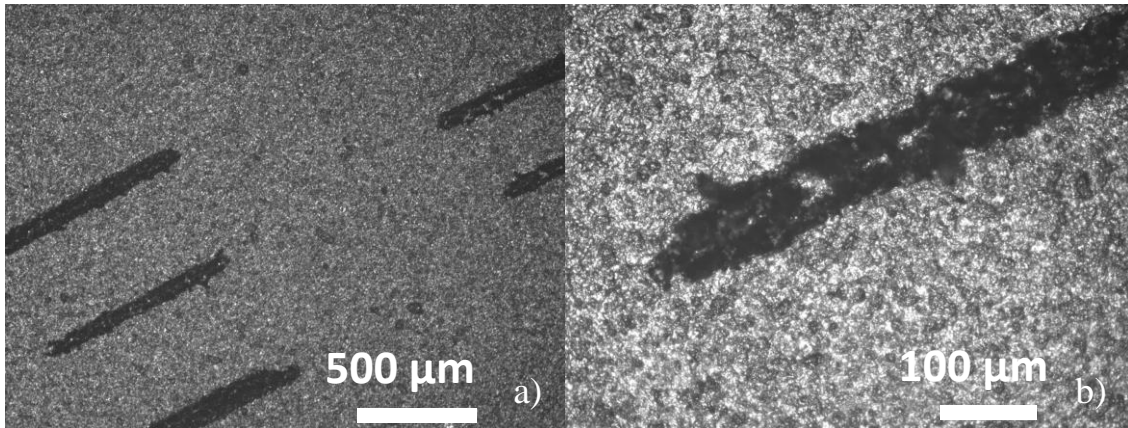


Figure 3.8 - a) Several laser traces thicknesses ranging from 0.01 mm to 0.1 mm with a step of 0.1 mm at 5% power b) smallest thickness well defined with a 5% power.

3.2 Capacitors

After determining the best laser parameters for obtaining optimized rGO layers, these were used to perform different geometries capacitors. Images of the capacitors' geometries are shown in Figure 3.9. These geometries were tried according to the literature best geometry. [28]

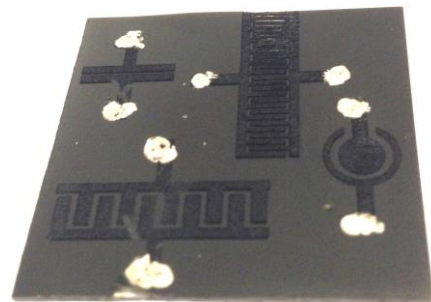


Figure 3.9 - Geometries of the tested capacitors.

3.2.1 Geometry influence

The four geometries tested were laser printed and the cyclic voltammetry curves were plotted, as showed in Figure 3.10.

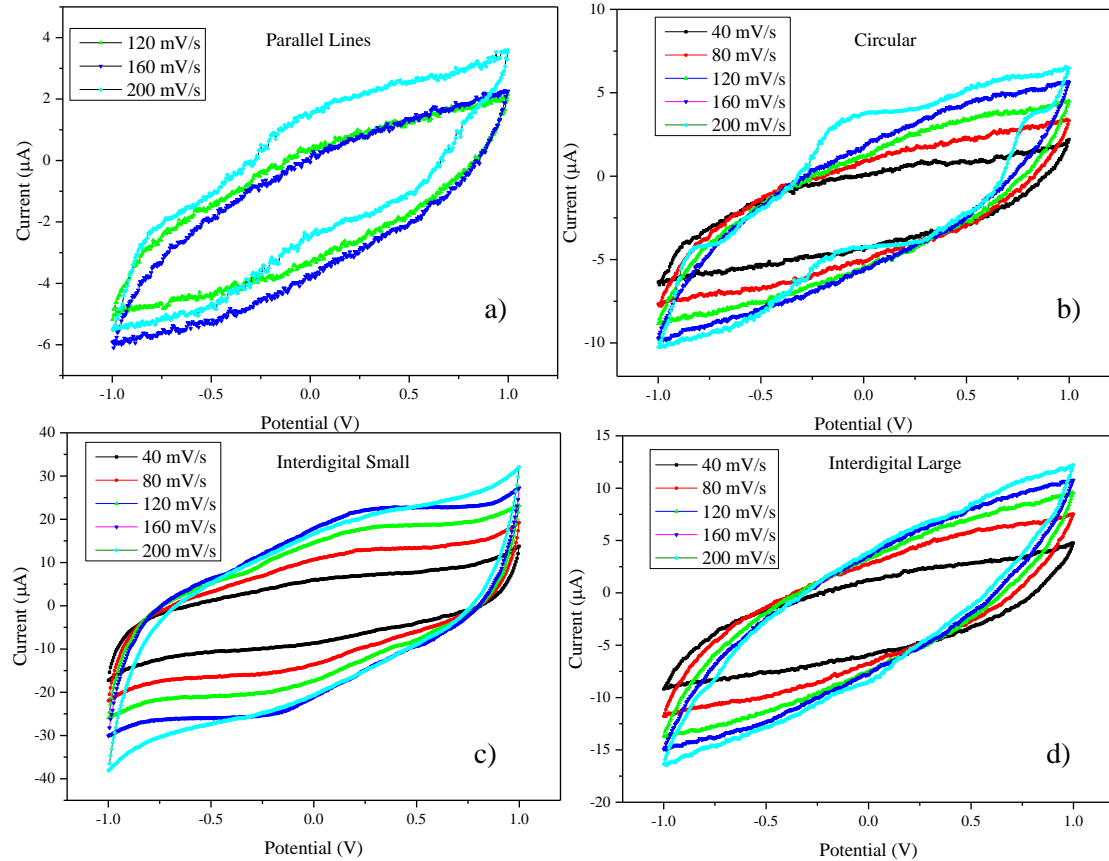


Figure 3.10 - CV curves of the four different geometries: a) Parallel Lines, b) Circular, c) Interdigital Small and d) Interdigital Large.

The parallel lines, show the lowest specific capacitance of all four. For the two first scan rates, 40 mV/s and 80mV/s, it was not possible to extract a value since the current of the device analysed is less than the limit of detection of the potentiostat used. The curves presented in Figure 3.10 a) and b) do not show a symmetry in the current values as it happens for high quality capacitors. This can be due to series resistance since it is in the hundred ohms' range.

Curves b) and c) shows some accumulation and reduction behaviour together with some current losses which can be explained by recombination of charges into defects existent in rGO and also because a limited surface area for accumulation due to the geometry used.

Curves c) and d) shows almost the same values at both ends, no matter the axis, and an increase from one scan rate to the next, as one would expect. The interdigital electrodes are more stable than the other two, being the curves of the smaller more rectangular-like shape and showing higher currents. To test this hypothesis, the specific capacitances of devices have been calculated

using the Gamry Echem Analyst software. The results were divided by the contact area of the device allowing a direct comparison value.

Analysing Table 3.3, an almost obvious decrease in value can be detected with the increase of the scan rate. In theory, the current detected increase proportionally with the scan rate, meaning that if the scan rate is doubled the current measured should double too. With the devices created this not happen, probably due to a lack of equilibrium in the device for greater speeds. The meaning is, with the increase of scan rate, slower reactions do not have enough time to reach an equilibrium.

The circular shape assumes a better performance in stability, showing a difference between the highest and the smallest specific capacitance of $18.7 \mu\text{C}/\text{mm}^2$. However, the highest results were obtained by the interdigital with smaller gaps between the fingers, almost the double for lower scan rates and a negligible decrease for the fastest scan rate, comparing to the circular or parallel lines.

Table 3.3 - Influence of the geometry in the specific capacitance of the device with different scan rates (capacitance in $\mu\text{C}/\text{mm}^2$).

<i>Scan Rate mV/s</i>	40	80	120	160	200
<i>Interdigital Small</i>	109.7	99.2	88.5	78.4	56.5
<i>Interdigital Large</i>	66	68.6	55.4	46.2	39.1
<i>Circular</i>	48.4	66.6	67.1	65.9	64
<i>Parallel Lines</i>	N/A	N/A	40.9	26.8	61.6

3.2.2 Electrolyte influence

In order to test the electrolytes produced, 15 devices were printed, 3 for each electrolyte and 3 for a base line. In this test, small strips of carbon tape were placed in the contacts of the interdigital supercapacitor to reduce the influence of the in-series resistance and test only the electrolyte in use. The base line, Figure 3.11, shows irregularities along the curve, noise derivative

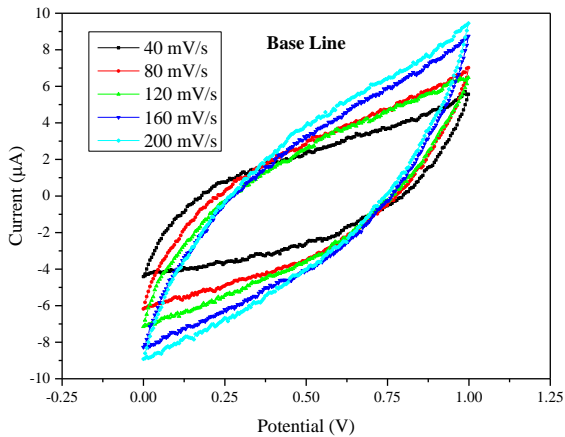


Figure 3.11-CV curve of base line without electrolyte.

from the proximity to the lower resolution of the potentiostat. The curves are almost evenly spaced, representing a good relation between the scan rate and maximum current. The shape of the plots represents an important aspect, ideally being a more rectangular shape with two round edges. The curves in Figure 3.11 assumes a more elongated shape, probably due to in-series resistance that is being added to the device.

Development of Graphene Based Supercapacitors

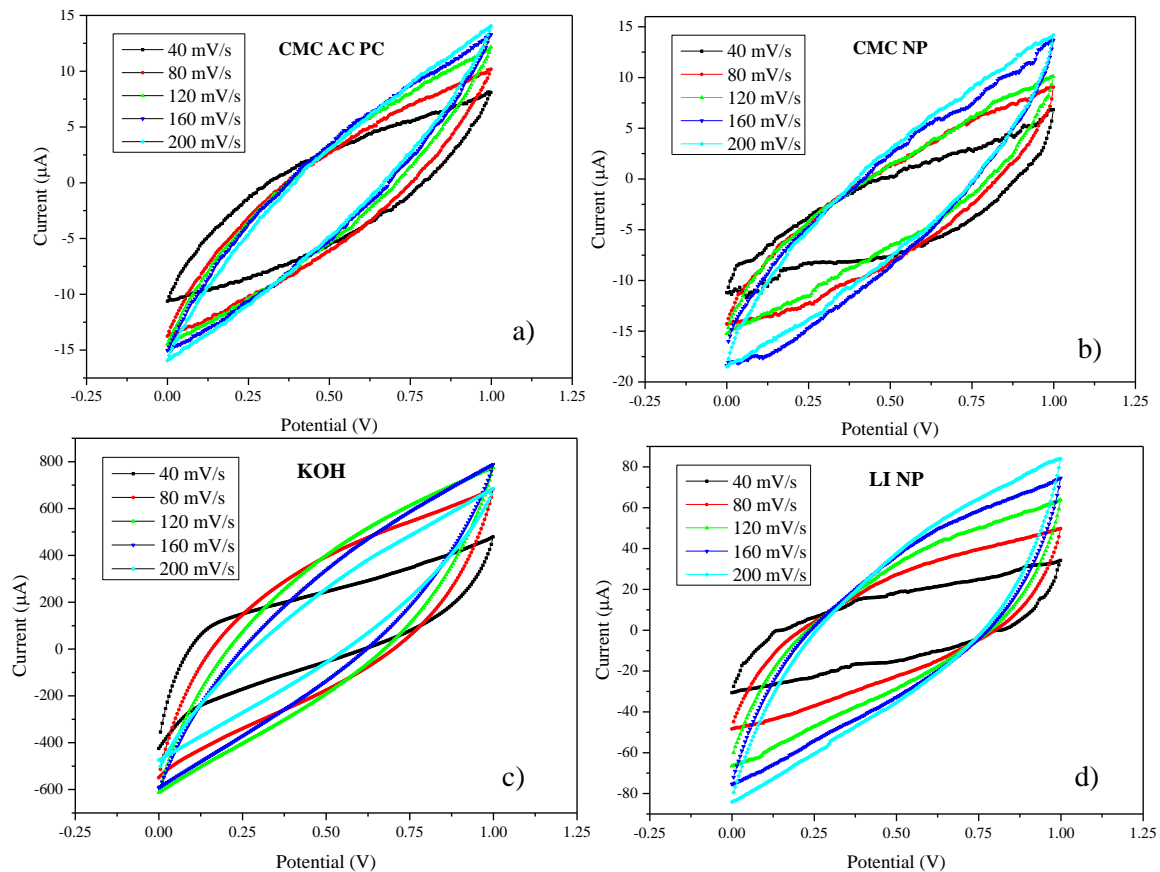


Figure 3.12 - CV curves of each electrolyte used: a) CMC AC PC; b) CMC NP; c) KOH; d) IL NP.

In the plots of Figure 3.12, are shown more stable and symmetrical CV. Comparing to the base line, Figure 3.11, the CMC with NP of SiO₂ demonstrate a more instable symmetry, showing an intense peak at negative current and several small distortions along the curve, probably due to the solid state of the electrolyte. The curves for electrolyte CMC with AC-PC, show a much more stable IV curves but with overlapping of each scan rate. This means that, at higher scan rates, the ions in the electrolyte does not have enough time to establish and reach equilibrium. The specific capacitance, as it is divided by the scan rate, decreases when the scan rate rises and therefore results show instabilities.

In Figure 3.12 c) the IV plots for KOH electrolyte shows a much higher current than any other electrolyte tested. The smallest scan rate, 40mV/s, have a rectangular-like shape more defined than the others, but, just as CMC AC PC, the other 4 scan rates are almost overlapping each other, which indicate a non-linear relation between scan rate and the height of the current curve. The IL NP, plotted in Figure 3.12 d), have a better relation but with the drawback of one order of magnitude lower in the maximum peak of the current. This can be related to the size of each ion. The bigger ion present in the IL makes diffusion in the electrode much harder and slower than its counterpart, contributing to a slower movement of ions in the electrolyte.

The complete results can be observed in Table 3.4 and, as someone might expect, all electrolytes improved the base line, except the CMC NP in two scan rate. This is probably justifiable with a low charge movement of the solid-state electrolyte, since CMC AC PC also shows small improvement of the base line.

Table 3.4 - Test results of the electrolytes at different scan rates (capacitance in $\mu\text{C}/\text{mm}^2$).

<i>Scan Rate mV/s</i>	40	80	120	160	200
<i>Without Electrolyte</i>	50.29	45.75	23.91	22.82	20.82
<i>CMC AC PC</i>	116.76	73.03	38.02	45.72	39.30
<i>CMC NP</i>	19.13	29.90	25.87	24.76	22.52
<i>KOH</i>	7389.37	5040.35	4310.84	2841.5	1981.91
<i>IL NP</i>	499.84	258.96	228.84	204.62	173.38

Overall, the solid-state electrolytes allow to make a full solid device but with a much lower specific capacitance. On the other hand, the liquid electrolyte gives a higher specific capacitance but requires an enclosure to make sure the it stays in the device. The KOH evaporates from the device along the time, which does not happen to the ionic liquid and therefore depending exclusively in the application and necessities for the device, the most appropriate electrolyte can be chosen.

The plot in Figure 3.13 shows the stability of every electrolyte with the variation of the scan rates. The CMC AC PC presents the same oscillation in the specific capacitance as the base line and, therefore, indicating a possible correlation between the two. The drops of the liquid

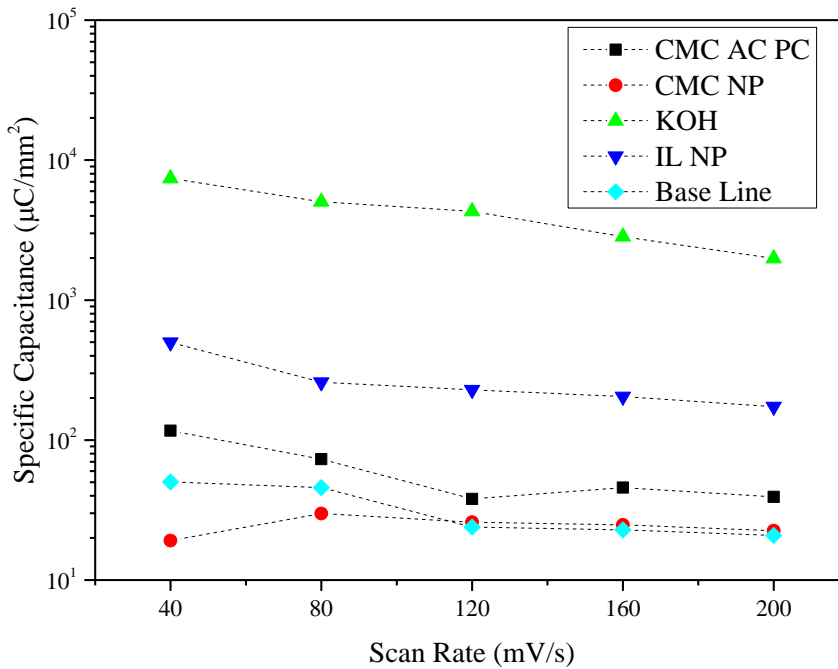


Figure 3.13 - Specific Capacitance of every electrolyte vs scan rate.

electrolytes values are almost identical, possibly due to the phase of the electrolyte itself but the solid electrolytes seem to have a better stability, notwithstanding the lower values.

Due to the expected stability of IL NPs electrolyte, the device made with it was re-measured after a month storage in room air conditions.

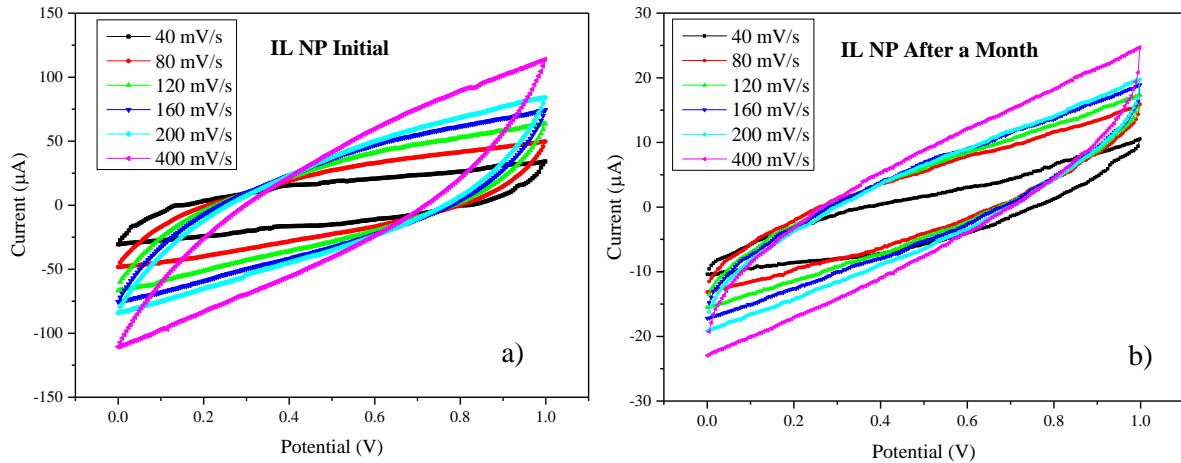


Figure 3.14 - IL NP CV curves a) Initial b) after a month.

As seen in Figure 3.14, the decrease is huge. Almost 80% of the initial specific capacitance was lost. This is probably due to a migration of the electrolyte to the contacts and even to the rest of the film, meaning that some sort of enclosure or protection have to added to the device to prevent this from happening.

3.3 Electrochemical synthesis

Since the production of graphene via GO is expensive and environmentally unfriendly, in this work another way to produce it was tested and characterized. The electrochemical synthesis was tried with different medium concentration: sea water; and 0.1M; 0.3M; 0.5M Na_2SO_4 being the graphite source a commercial graphite rod. The Raman spectra of the obtained powder after being washed to remove excess of salt are shown in Figure 3.15. The spectrum of graphite powder from the initial rod is included for comparison purposes.

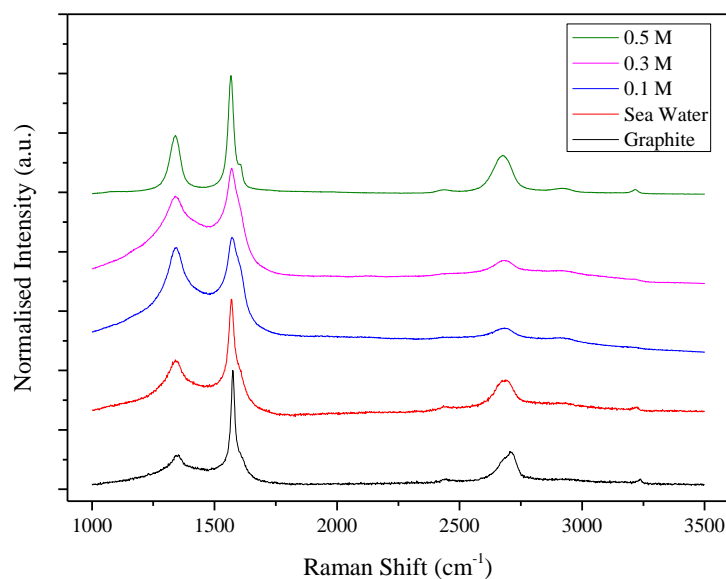


Figure 3.15 - Raman shift of the Electrochemical synthesis's powders obtained with sea water and Na_2SO_4 solutions of 0.5M; 0.3M; and 0.1M.

A clear left shift is visible in the 2D band of all electrochemical samples. This shift can indicate an effective exfoliation because, as showed in the literature, graphene-like materials shows a similar shift comparative to graphite.[34] In Table 3.5, can be notice that the most left shifted 2D belongs to the solution of 0.5M Na_2SO_4 , and that can possible be an indicator of an increase of surface area and, therefore, a better approach to graphene.

Table 3.5 – Raman Shift Peaks of all samples (peak position in cm^{-1}).

	D	G	2D
<i>Graphite</i>	1343	1574	2712
<i>0.1M</i>	1345	1571	2682
<i>0.3M</i>	1340	1570	2682
<i>0.5M</i>	1340	1566	2676
<i>Sea Water</i>	1340	1569	2685

To explore this hypothesis, the peaks' heights were plotted and displayed in the Figure 3.16. As said before, this information is subjective due to analysis being made in a laser focus point. This meaning that the height of the peaks can change from one focus point to another, making definitive conclusions draw from this susceptible to further confirmation. The I_D/I_G ratio decreases with the increase of the salt concentration. This is expected due to the type of technique used. As salt infiltrate the graphite, small fragments of material release from the original rod

Development of Graphene Based Supercapacitors

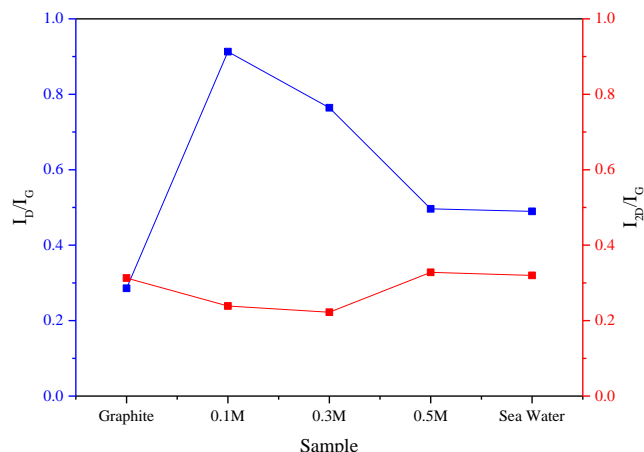


Figure 3.16 - Raman spectra's ratios for each Electrochemical sample and the initial graphite.

creating more defects in the frontiers of the particles. It can also be seen that this ratio decrease to the higher level of salt, probably because the pieces that get out of the graphite rod are bigger. The sea water, surprisingly, shows almost the same results as the higher concentration of Na_2SO_4 for both ratios. However, this could imply a simple aggregation or bigger particles and a lower number of defects.

The deconvolution of 2D bands was performed. The graphs of this deconvolution are shown in Figure 3.17, being the peaks fitted by a Lorentzian function.

In Figure 3.17 a), the 2D peak of the starting graphite can be seen and, as expect, can be deconvolution in smaller curves using a Lorentz fit. This possibility of deconvolution indicates a higher number of layers which, again, was expected from the starting graphite. This will serve as a base line for all the samples, as if the material produced only require one peak for a perfect fit, the material is better exfoliated and reassembles more with graphene.

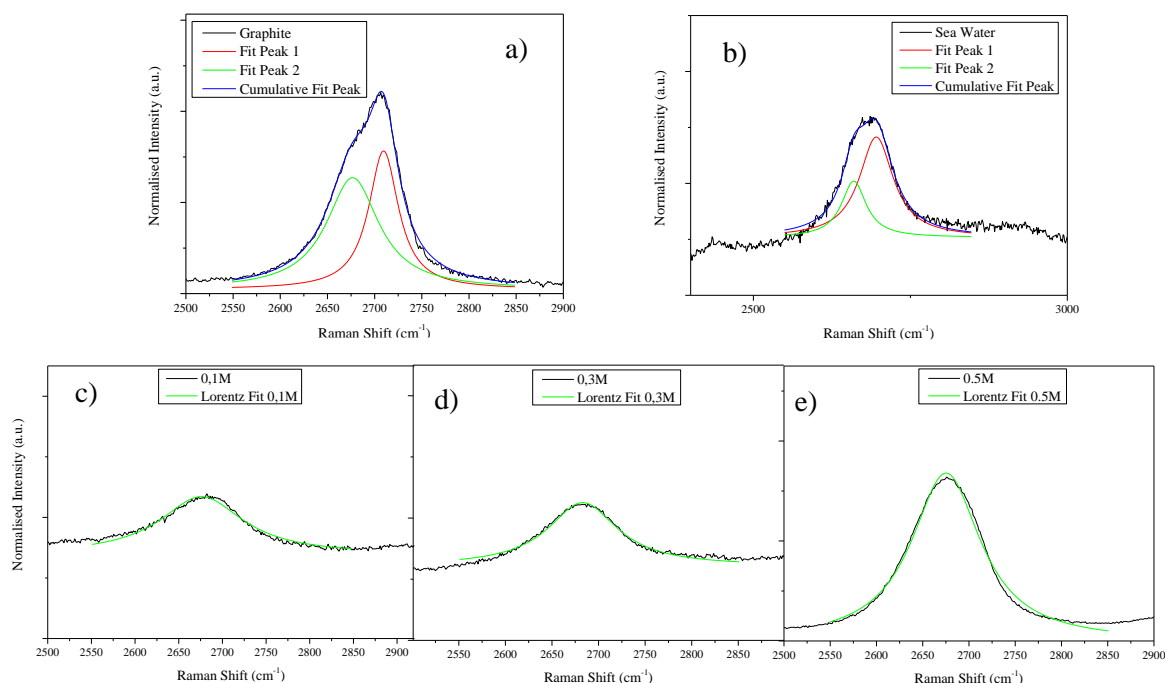


Figure 3.17 - Deconvolution of Raman Spectra 2D peaks through Lorentz Fit of powder created from: a) Starting Graphite; b) Sea Water; c) 0.1M; d) 0.3M; and e) 0.1M.

The deconvolution of the 2D bands of the Na_2SO_4 solution products' 2D band can be observed in Figure 3.17 c) d) and e) and conclusions can be taken. All the bands can be fitted with an only curve, meaning that any of them have fewer layer than the starting graphite, as said in the literature. [34]

In the Figure 3.17 b), the sea water sample's 2D peak can be observed deconvoluted and a contribution from two peaks is obvious. This means that even with a similar result in the ratios of the peaks as 0.5M of salt, the sea water solution result in more layers' powder and, therefore, a worst exfoliation than the Na_2SO_4 salt.

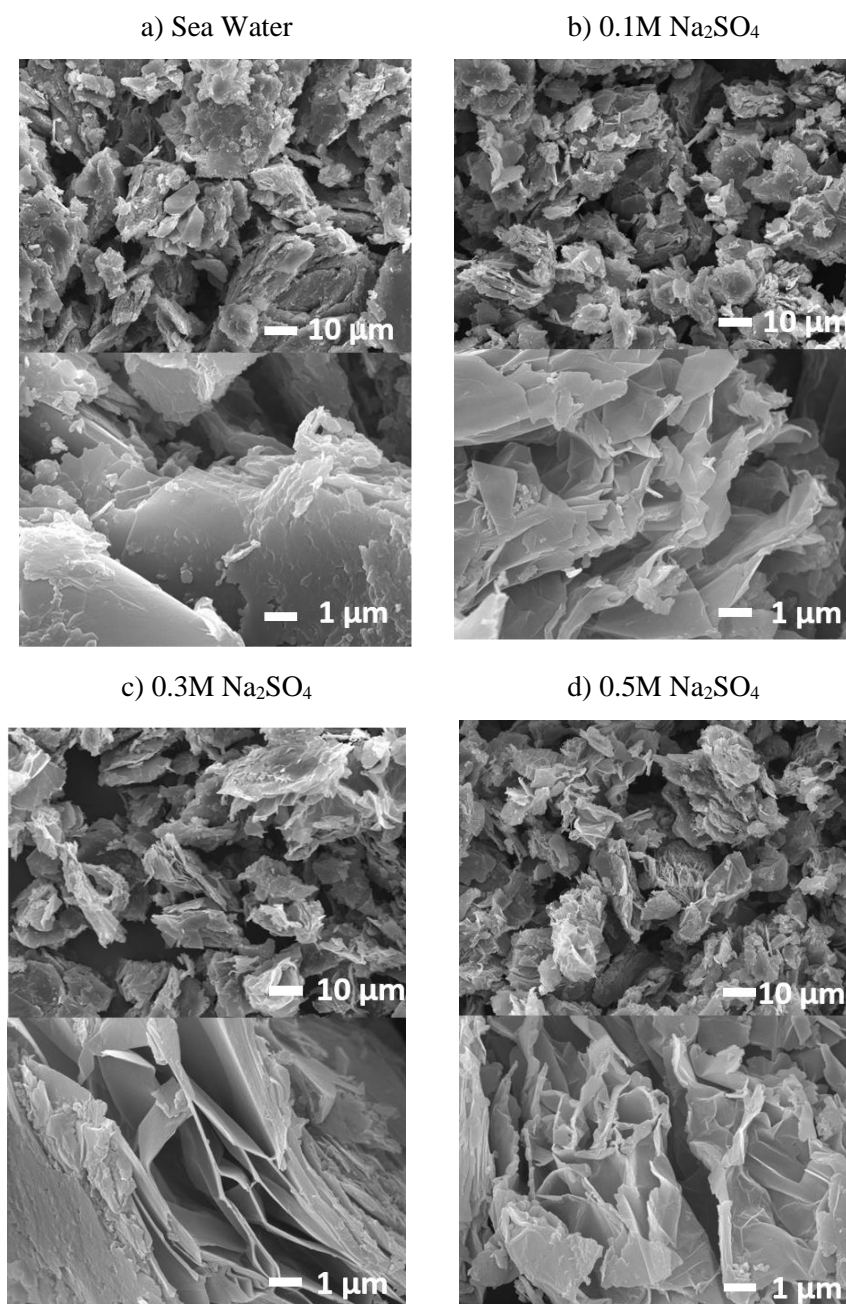


Figure 3.18 - SEM images of the powders produced

From the SEM images, Figure 3.18, in all lower magnification scales, 10 μm , are seen huge blocks of material forming a not so even powder, with a large range of particles size. To discuss the effectiveness of the exfoliation, the smaller scale is required.

In the electrochemical exfoliation with sea water, the powder produced shows compact blocks formed by nanometric sheets that are bonded to each other. This may indicate a fragmentation of the graphite and not a graphite layers' exfoliation into graphene.

The samples obtained from Na_2SO_4 solutions at microscale are all formed by flakes with variable sizes. However, at nanometric scale all samples show separated sheets. It is noticeable, that with the increase of the salt concentration, the exfoliation and dispersion of sheets is enhanced.

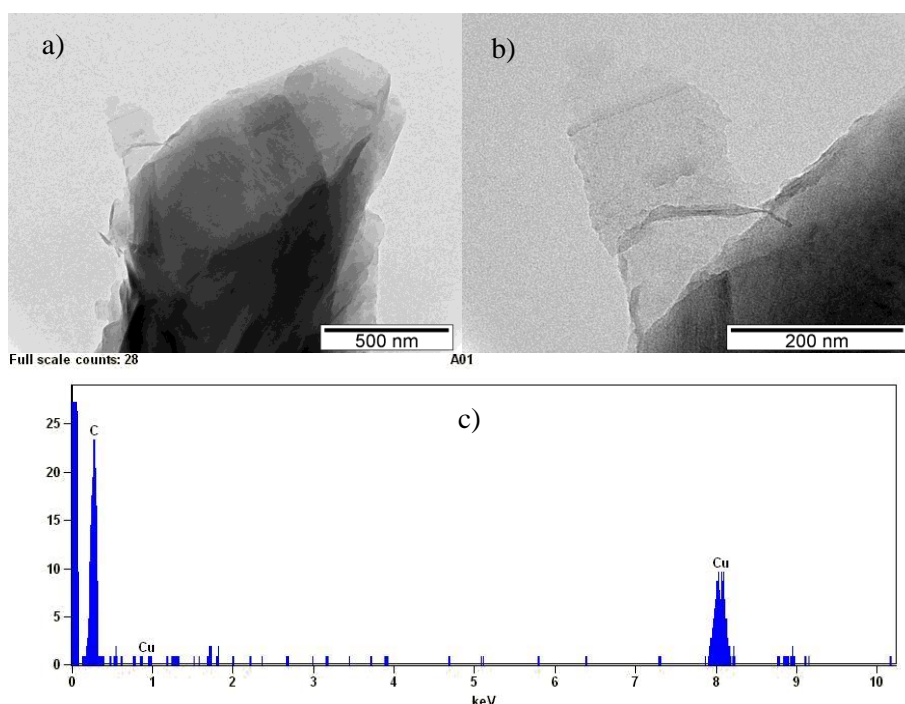


Figure 3.19 – a) and b) TEM images with different magnification, of exfoliated powder with 0.1M Na_2SO_4 solution c) EDS analysis of the same powder.

Using dispersions in ethanol of the powders produced, a small drop was placed in a TEM grid and the images observed. A single flake of the 0.1M Na_2SO_4 solution's products can be observed in Figure 3.19 a), where multiple sheets are seen. On larger magnification image, 200 nm, a single sheet of graphene is detected. No impurities can be found and, to confirm it, EDS analysis was performed. The result shown in Figure 3.19 c) reveal an absolute peak of carbon from the graphene-like material and peaks from copper which are attributed to the TEM grid. This is a good indication that all the salt used was washed away and the powder created remained all carbon with no contamination whatsoever.

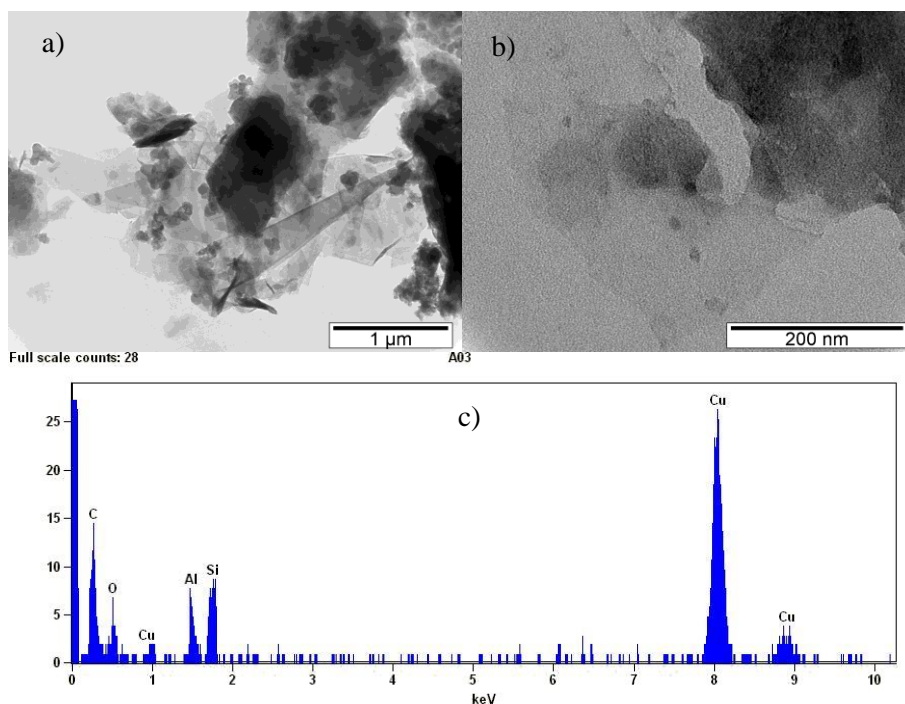


Figure 3.20 - a) and b) TEM image of exfoliated powder with 0.3M Na_2SO_4 solution
c) EDS analysis of the same powder.

The same cannot be said about the powder obtained for higher concentrations of Na_2SO_4 . In Figure 3.20, the TEM image shows agglomerates of sheets and impurities are also present. Even so, the smaller scale, although out of focus, displays a thin sheet of material indicative of a good exfoliation and possible larger area of the sheets.

Through the EDS analysis, it is possible to observe an aluminium and silicon contamination. This is explained by the salt used to exfoliate the graphite. One possibility is that Na_2SO_4 aqueous solution could etch glass and, since the experiment was conducted in a glass goblet, some particles of it could end up in the powder, resulting in the contamination. It is also visible an oxygen peak that could be a remnant of the salt or even an oxidation occurred in the exfoliation process or from silica. The copper peaks, as said before, belongs to the sample grid used to handle the powder inside of TEM equipment.

The 0.5M of salt samples shows even larger foils but also more irregularities than the previous two. In Figure 3.21, the biggest scale shows a complex furl of sheets and, therefore, less visible single sheets. With a magnification to the top right corner, overlapping sheets can be seen with some contamination. This stains elements can be seen through the EDS analysis, where two new peaks appear, comparative with the previous one, Na and S. This confirm the hypothesis that some of the salt stayed in the powder. Giving the fact that all the samples received the same

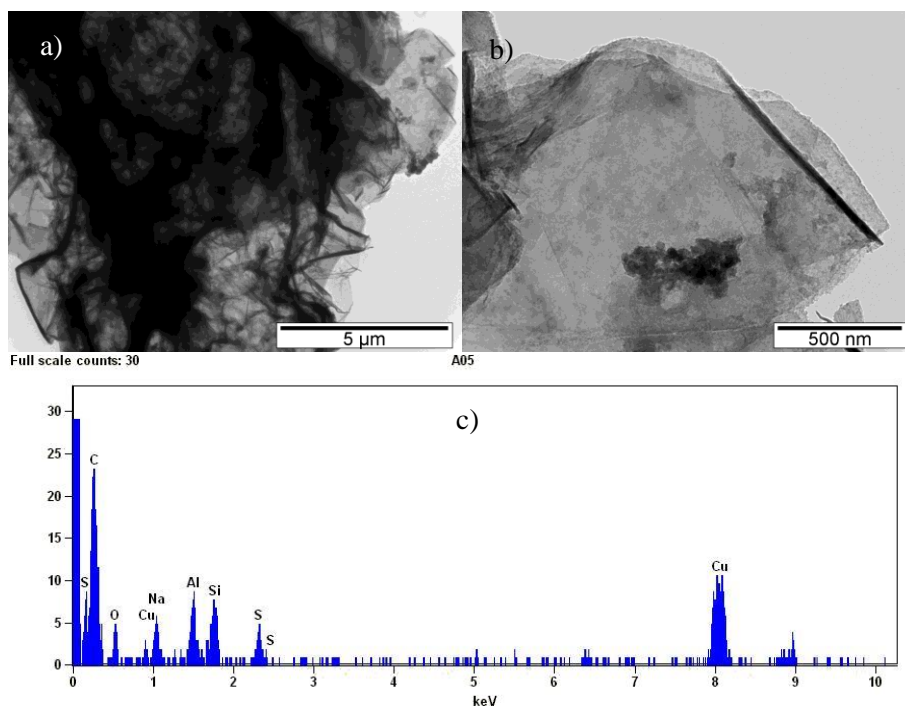


Figure 3.21 - a) and b) TEM image of exfoliated powder with 0.5M Na_2SO_4 solution
c) EDS analysis of the same powder.

number of washes cycles, it is predictable that, if one of them have presence of salt, the sample with the higher concentration exhibit bigger peaks. This is confirmed in this experience, the higher the salt concentration in the solution, the bigger is the presence of salt in EDS spectra. To eliminate its presence, the number of wash cycles needs to be adjusted to the concentration in use. The aluminium silicate can be eliminated with the use of different goblet such as Teflon. Using the two amendments to the procedure, is expected an increase in purity of the powder or, at least, a minimization of this contamination and obtaining of a pure carbon powder.

However, the obtained results confirm the possibility to obtain few layer graphene from graphite exfoliation by a simple electrochemical process. In further studies techniques, such as XPS, will help to confirm the type of predominant bonds.

4 Conclusions and Future Perspectives

Laser reduction of GO was obtained with success. Of the three parameters studied, two show no necessity of fine tuning and represent negligible differences between samples in the range studied. Frequency and speed shows little variations of conductivities and with small discrepancies in the Raman ratios. Nevertheless, the Raman spectra of all samples showed a decrease in the number of defects and an arising of the 2D band, indicating a successful reduction of the film into rGO. Power, on the other hand, proves to be a key factor to insure a better reduction. The conductivities of the P4 and P7 proven the visual conclusion from the microscope image, producing a less uniform film and therefore less conductor. The Raman spectra for each of these samples still shows signs of a reduction but micro Raman analyses is punctual and the film could be non-uniform. For the other two powers, P5 and P6, all tests were inconclusive in attributing a better reduction. Raman spectra showed the same peaks of the other samples, proving the reduction and, with no further research, the more energetic efficient P5 condition was chosen as the best option. In a further study, a design of experiment could be done to test the interdependence of the parameters.

The 4 device's geometry tested presents conclusive results in its capacitance and stability. Parallel lines show the worst result, with two of the scans rates' curves below the limit of detection of the potentiostat used. The circular geometry assumes the best stability, with small variation in the results. The highest value for the specific capacitance were obtained by the interdigital with small spacing between the fingers at the slower scan rate, 40 mV/s, with a value of 109.7 $\mu\text{C}/\text{mm}^2$. A further optimization of spacing between fingers and its relation to their size, would improve the specific capacitance of the devices.

From the solid electrolytes studied, only CMC AC PC have improved the specific capacitance compared to the one obtained without electrolyte. It doubles in almost every scan rate tested obtaining the best result for the slower scan rate with an increase over 200%. The CMC NP solid electrolyte did not improve the device, probably due to a low ion conduction that could be confirmed using techniques such as Electrochemical Impedance Spectroscopy. On the other hand, liquid electrolytes greatly enhance the capacitance, it is 1000% enhanced with IL NP reaching, with the KOH, 7389 $\mu\text{C}/\text{mm}^2$ for the slower scan rate. This was the best result obtained.

On this work was proven that it is possible to achieve few-layers graphene using methods and techniques much more environmentally friendly and cheaper than the conventional chemical routes. The powders produced were characterized by Raman, SEM and TEM and the results demonstrate a proper exfoliation of the graphite rod used in the electrochemical process. A clear

red shift from the starting graphite 2D band is visible in all samples of electrochemical produced powders and, according to the literature, the result is the one expected from few-layers graphene. This result was supported by the SEM images of the powders, where nanosheets are presented. There is also possible to observe a relation between the salt concentration and the exfoliation of the powder. With the increase of this parameter, the samples show more and thinner sheets, rising the superficial area.

The TEM images of the same powders shows undoubtedly nanosheets, although with some impurities. Using the complementary EDS analysis, a correlation between the salt concentration and the presence of oxygen and sodium contamination is observed, meaning that more wash cycles is necessary to improve the purity of the powder. Another contamination found in the higher concentrations is an aluminum silicate, indicating a possible etch from the glass goblet used in the electrochemical process. To improve this process a Teflon goblet could be used and eliminate this impurity.

The primary objectives of this work were accomplish. The devices were created using the laser parameters optimized and an attempt to create an all-solid-state device result in an enhancement, with room for further improvements. The electrochemical synthesis produces few-layers graphene and, since it was proved that displays a higher surface area, could be applied in supercapacitor in future works.

References

- [1] A. González, E. Goikolea, J. A. Barrena, and R. Mysyk, “Review on supercapacitors: Technologies and materials,” *Renew. Sustain. Energy Rev.*, vol. 58, pp. 1189–1206, 2016.
- [2] K. S. Novoselov, V. I. Fal'ko, L. Colombo, P. R. Gellert, M. G. Schwab, and K. Kim, “A roadmap for graphene,” *Nature*, vol. 490, no. 7419, pp. 192–200, 2012.
- [3] I. Childres, L. Jauregui, W. Park, H. Cao, and Y. Chen, “Raman Spectroscopy of Graphene and Related Materials,” *New Dev. Phot. Mater. Res.*, pp. 1–20, 2013.
- [4] M. J. Allen, V. C. Tung, and R. B. Kaner, “Honeycomb carbon: A review of graphene,” *Chem. Rev.*, vol. 110, no. 1, pp. 132–145, 2010.
- [5] Y. Zhu, S. Murali, W. Cai, X. Li, J. W. Suk, J. R. Potts, and R. S. Ruoff, “Graphene and Graphene Oxide: Synthesis, Properties, and Applications,” *Adv. Mater.*, vol. 22, no. 35, pp. 3906–3924, 2010.
- [6] M. Beidaghi and C. Wang, “Micro-Supercapacitors Based on Interdigital Electrodes of Reduced Graphene Oxide and Carbon Nanotube Composites with Ultrahigh Power Handling Performance,” *Adv. Funct. Mater.*, vol. 22, no. 21, pp. 4501–4510, 2012.
- [7] Y. J. Kim, Y. H. Kahng, N. Kim, J.-H. Lee, Y.-H. Hwang, M. Lee, S. M. Choi, W. B. Kim, and K. Lee, “Impact of synthesis routes on the chemical, optical, and electrical properties of graphene oxides and its derivatives,” *Curr. Appl. Phys.*, vol. 15, pp. 1435–1444, 2015.
- [8] B. Gadgil, P. Damlin, and C. Kvarnström, “Graphene vs. reduced graphene oxide: A comparative study of graphene-based nanoplateforms on electrochromic switching kinetics,” *Carbon N. Y.*, vol. 96, pp. 377–381, 2016.
- [9] M. Liang and L. Zhi, “Graphene-based electrode materials for rechargeable lithium batteries,” *J. Mater. Chem.*, vol. 19, no. 33, p. 5871, 2009.
- [10] Y. Liu, X. Dong, and P. Chen, “Biological and chemical sensors based on graphene materials,” *Chem Soc Rev*, vol. 41, no. 6, pp. 2283–2307, 2012.
- [11] W. Hong, Y. Xu, G. Lu, C. Li, and G. Shi, “Transparent graphene/PEDOT-PSS composite films as counter electrodes of dye-sensitized solar cells,” *Electrochem. commun.*, vol. 10, no. 10, pp. 1555–1558, 2008.
- [12] Q. Zhou, X. Ye, Z. Wan, and C. Jia, “A three-dimensional flexible supercapacitor with enhanced performance based on lightweight, conductive graphene-cotton fabric electrode,” *J. Power Sources*, vol. 296, pp. 186–196, 2015.
- [13] P. Kumar, F. Shahzad, S. Yu, S. M. Hong, Y.-H. Kim, and C. M. Koo, “Large-area reduced graphene oxide thin film with excellent thermal conductivity and electromagnetic interference shielding effectiveness,” *Carbon N. Y.*, vol. 94, pp. 494–500, 2015.
- [14] K. S. S. Novoselov, A. K. K. Geim, S. V. V. Morozov, D. Jiang, Y. Zhang, S. V. V. Dubonos, I. V. V. Grigorieva, and A. A. A. Firsov, “Electric Field Effect in Atomically Thin Carbon Films,” *Science (80-.)*, vol. 306, no. 5696, pp. 666–669, 2004.
- [15] B. C. Brodie, “On the Atomic Weight of Graphite,” *Philos. Trans. R. Soc. London*, vol. 149, no. 9, pp. 249–259, 1859.
- [16] L. Staudenmaier, “Verfahren zur Darstellung der Graphitsäure,” *Berichte der Dtsch. Chem. Gesellschaft*, vol. 31, no. 2, pp. 1481–1487, May 1898.

- [17] J. William S. Hummers and R. E. Offeman, "Preparation of Graphitic Oxide," *J. Am. Chem. Soc.*, vol. 80, no. 1937, p. 1339, 1958.
- [18] D. A. Dikin, S. Stankovich, E. J. Zimney, R. D. Piner, G. H. B. Dommett, G. Evmenenko, S. T. Nguyen, and R. S. Ruoff, "Preparation and characterization of graphene oxide paper," *Nature*, vol. 448, no. 7152, pp. 457–460, 2007.
- [19] J. Kauppila, P. Kunnas, P. Damlin, A. Viinikanoja, and C. Kvarnström, "Electrochemical reduction of graphene oxide films in aqueous and organic solutions," *Electrochim. Acta*, vol. 89, pp. 84–89, 2013.
- [20] C. Gmez-navarro, R. T. Weitz, A. M. Bittner, M. Scolari, A. Mews, M. Burghard, and K. Kern, "Electronic Transport Properties of Individual Chemically Reduced Graphene Oxide Sheets," pp. 0–4, 2007.
- [21] M. Emre Ayhan, G. Kalita, R. Papon, R. Hirano, and M. Tanemura, "Synthesis of transfer-free graphene by solid phase reaction process in presence of a carbon diffusion barrier," *Mater. Lett.*, vol. 129, pp. 76–79, 2014.
- [22] Y. Xue, L. Zhu, H. Chen, J. Qu, and L. Dai, "Multiscale patterning of graphene oxide and reduced graphene oxide for flexible supercapacitors," *Carbon N. Y.*, 2015.
- [23] F. Wen, C. Hao, J. Xiang, L. Wang, H. Hou, Z. Su, W. Hu, and Z. Liu, "Enhanced laser scribed flexible graphene-based micro-supercapacitor performance with reduction of carbon nanotubes diameter," *Carbon N. Y.*, vol. 75, pp. 236–243, 2014.
- [24] A. Ambrosi and M. Pumera, "Electrochemically Exfoliated Graphene and Graphene Oxide for Energy Storage and Electrochemistry Applications," *Chem. - A Eur. J.*, vol. 22, no. 1, pp. 153–159, 2016.
- [25] M. Halper and J. Ellenbogen, "Supercapacitors: A brief overview," *Rep. No. MP 05W0000272*, ..., no. March, p. Report No. MP 05W0000272, 1-29, 2006.
- [26] M. Winter and R. J. Brodd, "What are batteries, fuel cells, and supercapacitors?," *Chem. Rev.*, vol. 104, no. 10, pp. 4245–4269, 2004.
- [27] A. M. Namsnyk, "A Survey of Electrochemical Supercapacitor Technology," *Electr. Eng.*, no. June, p. 122, 2003.
- [28] M. F. El-Kady and R. B. Kaner, "Scalable fabrication of high-power graphene micro-supercapacitors for flexible and on-chip energy storage," *Nat. Commun.*, vol. 4, p. 1475, 2013.
- [29] H. Fei, C. Yang, H. Bao, and G. Wang, "Flexible all-solid-state supercapacitors based on graphene/carbon black nanoparticle film electrodes and cross-linked poly(vinyl alcohol)–H₂SO₄ porous gel electrolytes," *J. Power Sources*, vol. 266, pp. 488–495, 2014.
- [30] P.-L. Huang, X.-F. Luo, Y.-Y. Peng, N.-W. Pu, M.-D. Ger, C.-H. Yang, T.-Y. Wu, and J.-K. Chang, "Ionic Liquid Electrolytes with Various Constituent Ions for Graphene-based Supercapacitors," *Electrochim. Acta*, vol. 161, pp. 371–377, 2015.
- [31] G. P. Pandey, a. C. Rastogi, and C. R. Westgate, "All-solid-state supercapacitors with poly(3,4-ethylenedioxythiophene)-coated carbon fiber paper electrodes and ionic liquid gel polymer electrolyte," *J. Power Sources*, vol. 245, pp. 857–865, 2014.
- [32] P. Venezuela, M. Lazzeri, and F. Mauri, "Theory of double-resonant Raman spectra in graphene: Intensity and line shape of defect-induced and two-phonon bands," *Phys. Rev. B - Condens. Matter Mater. Phys.*, vol. 84, no. 3, pp. 1–25, 2011.
- [33] R. Narula and S. Reich, "Double resonant Raman spectra in graphene and graphite: A two-dimensional explanation of the Raman amplitude," *Phys. Rev. B - Condens. Matter Mater.*

- Phys.*, vol. 78, no. 16, pp. 1–6, 2008.
- [34] Y. Hao, Y. Wang, L. Wang, Z. Ni, Z. Wang, R. Wang, C. K. Koo, Z. Shen, and J. T. L. Thong, “Probing Layer Number and Stacking Order of Few-Layer Graphene by Raman Spectroscopy **,” pp. 195–200, 2010.
- [35] Y.-H. Lin, C.-Y. Yang, S.-F. Lin, and G.-R. Lin, “Triturating versatile carbon materials as saturable absorptive nano powders for ultrafast pulsating of erbium-doped fiber lasers,” *Opt. Mater. Express*, vol. 5, no. 2, p. 236, 2015.